From irreversible transformation of VO2 to V2O5 electrochromic films

Issam Mjejri, Mathieu Duttine, Sonia Buffiere, Christine Labrugère-Sarroste, Aline Rougier

From irreversible transformation of VO_2 to V_2O_5 Electrochromic Films

Issam Mjejri, Mathieu Duttine, Sonia Buffière, Christine Labrugère-Sarroste† and Aline Rougier*

Université de Bordeaux, CNRS, Bx INP, ICMCB, UMR 5026, F-33600 Pessac, France
† CNRS, Univ. Bx , PLACAMAT UMS 3626, F-33600 Pessac, France
*Corresponding Author: aline.rougier@icmcb.cnrs.fr

KEYWORDS : Electrochromism, VO_2, memory effect, characterization

ABSTRACT: Since its discovery, electrochromism, known as a modulation of the optical properties under an applied voltage, has attracted strong interest from the scientific community and has proved to be of significant utility in various applications. Although vanadium dioxide (VO_2) has been a candidate of extensive research for its thermochromic properties, its intrinsic electrochromism has scarcely been reported so far. In this study, multi-electrochromism is described from VO_2 thick films. Indeed, VO_2 opaque film, doctor bladed from homemade monoclinic VO_2 powder, shows a pronounced color modulation from orange to green and blue associated with an amorphization-recrystallization phenomenon upon cycling in lithium-based electrolyte. The strong memory effect allows to follow the coloration mechanism by combining various *ex-situ* and *in-situ* characterizations addressing both structural and electronic aspects. Upon cycling the multi-chromism of VO_2 finds its origin in a transformation of VO_2 into orange-V_2O_5 on oxidation while in reduction the blue color lithiated state illustrates a mixed vanadium oxidation state.

INTRODUCTION

Electrochromism is a perceptible phenomenon in which a color change is observed as a response to a variation of electric potential [1-3]. This process involves redox reaction and concerns a wide variety of materials [4]. Electrochromic systems find applications in a variety of fields ranging from smart windows (transmission mode) [5] to displays (reflective mode) [6]. With the continuous development of inorganic electrochromic materials, many transition metal oxides, such as WO_3, NiO, TiO_2, Nb_2O_5, MoO_3 and their derivatives, have been studied[7-11]. Among them, vanadium oxides are of growing interest showing both anodic and cathodic electrochromism allowing a multi-color switch suitable for display. The vanadium element exists in several oxidation states, namely V^{3+}, V^{4+}, and V^{5+}, leading to the formation of several oxides with exciting properties but until now mainly V_2O_5 has been recognized for its electrochromic performances [12-16].

Vanadium dioxide exists in different polymorphic forms, such as VO_2(A), VO_2(B), VO_2(C), VO_2(D), VO_2(M), and VO_2(R) [17-18]. Among these polymorphs, VO_2(M) is widely studied due to the metal–semiconductor transition between VO_2(M) and VO_2(R) making it an attractive candidate for intelligent thermochromic windows or emissivity control for space applications [19]. In this work, it will be shown that, next to its thermochromic performances, VO_2 is characterized by unexpected electrochromic properties (color modulation between blue, green and orange) accompanied by structure change from VO_2 (M1) to V_2O_5 under applied voltage,. To our knowledge, literature on EC properties of VO_2 is scarce and reported in very few papers using transmittance data [20]. In particular, aiming at combining thermochromism to electrochromism in a single material, Khan et al. attributed the modulation of transmittance in VO_2 sputtered films cycled in lithium based electrolyte to the insertion reaction forming Li_xVO_2. However, no structural information were provided.

Following the same path of combining two chromogenic properties, namely thermochromism and electrochromism, in a single material, we re-investigate VO_2 by choosing to work on opaque films suitable for displays and coatings for IR furtivity or thermal control applications. VO_2(M1) powders were synthesized by polyol synthesis from ammonium metavanadate (NH_4VO_3) and ethylene glycol. Vanadium dioxide thick films deposited by doctor blading were cycled in lithium based ionic liquid and electrochromic performances in the visible region were systematically investigated. The strong memory effect, persistence of color while no potential is applied, in both the reduced and oxidized states allowed *ex-situ* characterizations combining several techniques, namely Grazing Incidence X-Ray Diffraction GIXRD, High Resolution Transmission Electron Microscopy HRTEM, X-ray Photoelectron Spectroscopy XPS, Electron Paramagnetic Resonance EPR, Nuclear Magnetic Resonance NMR and Energy Electron Loss Spectroscopy EELS.

EXPERIMENTAL SECTION

Synthesis

The synthesis of the VO_2 (M1) phase was carried out using the polyol process mixing ammonium meta vanadate NH_4VO_3 to ethylene glycol ($H_6C_2O_2$) as template, with a final treatment at 500 °C for 2 h under vacuum ($PO_2 \approx 2 \times 10^{-5}$ Pa) of the intermediate vanadylglycolate (VEG). Details of the synthesis and of the powders characterization are reported in our work published in the journal Inorganic Chemistry in 2017[21]. VO_2(M1) films were doctor bladed on In_2O_3:Sn/glass, ITO/glass. The film thickness, measured using a Dektak mechanical profilometer, was of about 1200 nm ± 40 nm.

Electrochromic measurements

Electrochemical measurements were carried out in a three electrodes cell configuration using a BioLogic SP50 potentiostat/galvanostat apparatus, VO_2 films on ITO/glass as working electrode, a platinum foil as the counter-electrode and Saturated Calomel Electrode, SCE (ESCE = 0.234 V/ENH as reference electrode). All the electrochemical measurements were performed at room temperature in lithium-based electrolyte, namely lithium bis-trifluoromethanesulfonimide (LiTFSI, Solvionic, purity > 99.99%) in ethylimidazoliumbis-(trifluoromethane-sulfonyl)-imide (EMITFSI), in a voltage window of -0.9 V and +1.9V with a scan rate of 20 mV/s. After application of specific potentials, VO_2(M1) films diffuse reflectance spectra were *ex situ* recorded using a Varian Cary 5000 UV-Vis-NIR spectrophotometer. Colorimetric parameters in the CIE L*a*b* colorimetric space were deduced. The optical contrast (ΔE*) between two color states was calculated using the equation: $\Delta E^* = [(L^*_1-L^*_2)^2+(a^*_1-a^*_2)^2+(b^*_1-b^*_2)^2]^{1/2}$

Films characterizations

The film structure was characterized by X-ray diffraction analysis (Philips PW 1820, PANalytical X'Pert instrument, 2θ range from 8 to 60° and $\lambda_{CuK\alpha1}$=1.54056 Å).

Grazing incidence small angle X-ray scattering analyses, on films were carried out with a high-resolution diffractometer Bruker D8 Discover (films, grazing incidence, and textures), with Cu radiation. The adjustment of the grazing angles, namely 0.5, 1 and 2 degrees identified the 0.5 degree angle as the most suitable giving higher intensity.

Surface composition of the films, and the variation of the oxidation number of the vanadium cations, in cycled films were deduced upon the electrochemical measurements, by *ex-situ* X-ray photoelectron spectroscopy (XPS). The VG ESCALAB 220i-XL apparatus allows an analysis of the 5 nm first nanometers in depth with a lateral resolution of 150 µm. A ThermoFisher Scientific K-Alpha spectrometer was used for surface XPS analysis of thin films. The monochromatized AlKα source (hν=1486.6eV) was activated with a spot size 200 µm in diameter. The full spectra (0-1320 eV) were obtained with a constant pass energy of 200 eV and high-resolution spectra with a constant pass energy of 40 eV. High resolution XPS spectra were quantified and fitted using the AVANTAGE software provided by ThermoFisher Scientific.

In order to characterize the film composition and structure identification, the EELS combined with transmission electron microscopy (TEM) was used. Scratched film mixed with ethanol was deposited on copper grids (200 mesh) coated with carbon formvar. Three calibration powders of homemade V_2O_5, VO_2 and V_2O_3 were utilized. In order to stabilize the measurement, a cryogenic sample holder (GATAN) was used (at N_2 liq. Temperature: -165 °C). Measurements were performed on high-resolution (gun field emission) transmission electron microscope (HRMET) JEOL 2200FS, operated at 200 kV with a punctual resolution of 1.9 Å, as well as an "Omega" in-column energy filter (GATAN) for EELS spectra with an energy resolution of 1 eV. The following conditions were chosen for the EELS spectra acquisition: illumination semi-angle α=1.4 mrad and collection semi-angle β=6.6 mrad, dispersion=60 µm/eV. The 0-loss was acquired in 0.02 s and the V-(L_3-L_2) / O-K were acquired in 3 s (energy shift of +550 e V). An average of 7 or 8 different locations were recorded for each sample leading to homogeneous results (for V-(L_3-L_2) and O-K edges).

Electron Paramagnetic Resonance (EPR) spectra were recorded at room temperature with a Bruker ESP300E spectrometer operating at X-Band frequency (9.54 GHz). The main parameters used to characterize the scratched films are the following: microwave power 10 mW, magnetic field modulation frequency and amplitude 100 kHz and 0.4 mT, respectively and a spectral resolution of 0.3 mT.

^{7}Li Solid-State Nuclear Magnetic Resonance (SS-NMR) experiments were performed on a Bruker Avance III 300WB spectrometer (B_0 = 7.1 T, Larmor frequency of ^{7}Li: 116.6 MHz) equipped with a DVT BL2.5 magic-angle spinning (MAS) probe. The spectra were acquired using a Hahn echo (π /2 - π) pulse sequence synchronized to one rotor period (MAS rate: 30 kHz) with a π /2 pulse length of 2.0 µs and an optimized recycle delay of 1 s. A molar solution of LiCl ($\delta(^7Li)$ = 0 ppm) was used as external reference.

RESULTS AND DISCUSSION

Structural and morphological characterizations

VO_2(M1) powders were synthesized using the polyol process starting from a mixture of ammonium metavanadate and ethylene glycol forming a vanadyl glycolate VEG upon reaction. All the peaks of the X-ray patterns of the dark blue powders obtained by coprecipitation were indexed in the VEG phase (00- 049-2497 JCPDS data file; C2/c space group) (**Figure 1a**). The VEG powders were annealed under vacuum (2.10^{-5} Pa) for 2 h at 500 °C. After calcination (**Figure 1b**), the the narrowness of the peaks indicate an oxide with high crystallinity. The d-spacing values of all diffraction peaks match the ones of the monoclinic crystalline phase VO_2 (Space Group: P21/c) with lattice constants a = 3.564 Å, b = 11.510 Å, and c = 4.373 Å (JCPDS # 85-0601).

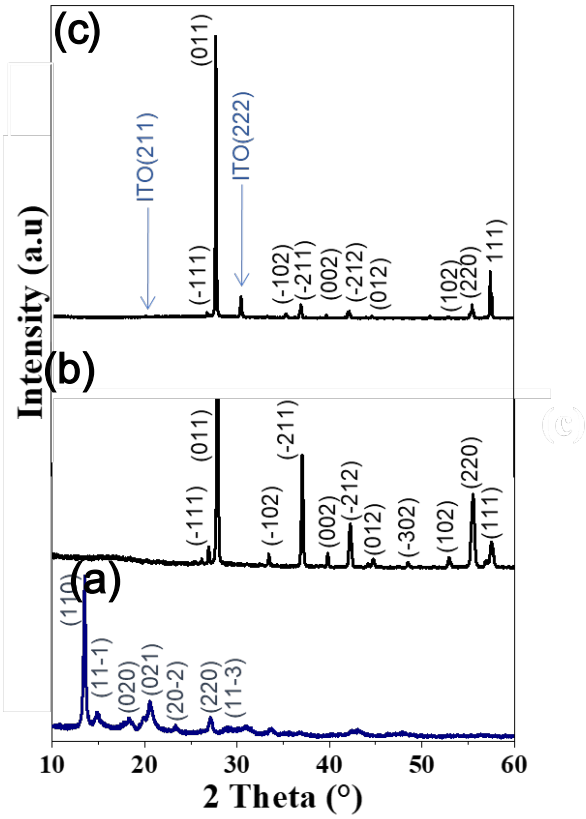

Figure 1. X-ray diffraction patterns of the (a) as-synthesized VEG (b) VO_2(M1) obtained at 500 °C post-treatment under vacuum (2.10^{-5} Pa) and (c) VO_2(M1) films.

From the as-synthesized VO_2(M1) powders, micrometer-thick electrochromic films (1.2 µm) were deposited on indium tin oxide (ITO) substrate using doctor blade technique. In first approximation, the XRD pattern of the as deposited opaque film shows similar features as the VO_2 powder **(Figure 1c)**. All the d-spacing values of the diffraction peaks (besides the ITO ones) match the ones of the monoclinic crystalline phase. Nonetheless, a preferential orientation along the (011) crystallographic direction of the VO_2 (M1) film was evidenced indicating that the associated lamellar morphology may be favoured by the coating process[22]. Indeed, a drastic evolution of the morphology from powder to film is observed for VO_2 (M1) from spherical powders to veil-shaped morphology **(Figure 2)**. As expected, the deposition method plays a significant an role on the surface morphology of VO_2 films [23,24].

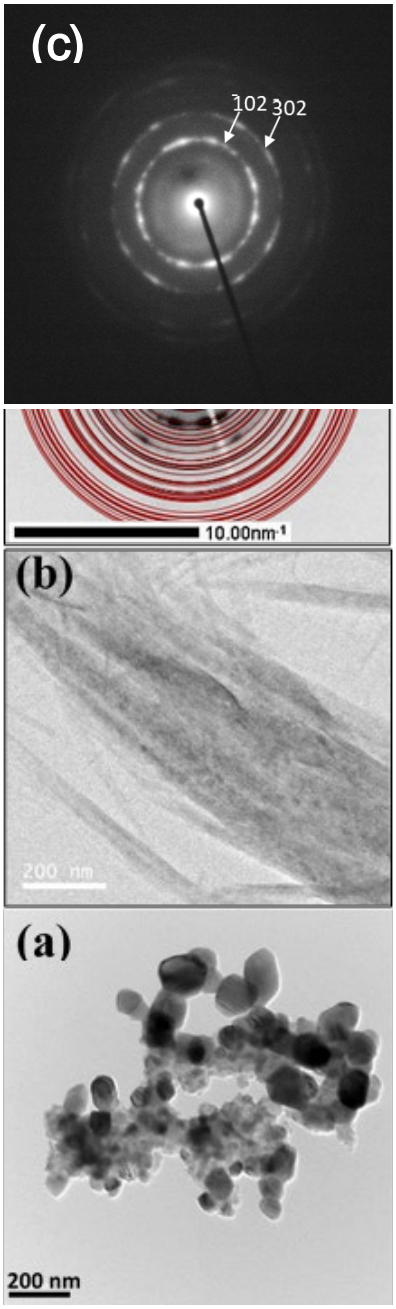

Figure 2. High-resolution images of VO_2(M1) (a) powders, (b) film prepared by doctor blading, (c) and corresponding electron diffraction pattern (of b).

For the as-deposited film, the electron diffraction pattern **(Figure 2c)** clearly shows the presence of dark spots which can be indexed to VO_2(M1) monoclinic phase according to the literature in good agreement with the XRD results.

Electrochromic characterization

The electrochromic activity of VO_2(M1) films was recorded in a lithium-based ionic liquid electrolyte. **Figure 3a** shows the 1st, 20th and 50th cyclic voltammograms (CVs) of the VO_2(M1) film deposited onto ITO and cycled, at a scan rate of 20 mV s^{-1} in the potential range of −0.9 to 1.9 V, in a three electrodes cell using ionic liquid based (0.3 M) LiTFSI in EMITFSI as a supporting electrolyte and Satured Calomel Electrode (SCE) as reference electrode. The CV shape clearly evolves upon cycling, both cathodic and anodic parts progressively becoming smoother and broader. Indeed, the first reductive scan shows two well defined peaks (at -0.2 V and -0.7 V), that progressively shift and broaden to merge into one large peak at about -0.5 V after 50 cycles and the oxidative wave gradually extends to higher voltage upon cycling. Nonetheless, the cyclic voltammetry of VO_2 films exhibit a good reversibility and stability in terms of capacity as illustrated by repetitive cycling, up to 500 cycles associated with no further evolution in the CV shape **(Figure S1)**. In agreement with a nice reversible process, the charges deduced from the CVs in reduction and in oxidation are very close showing however a slight decrease upon cycling (Figure S2). Such reversibility, may be surprising as it concerns an irreversible process on early cycling thus probably illustrating a continuous and progressive transformation. The number of cycles required for a complete VO_2 to V_2O_5 transformation still needs to be better evaluated. However, one can notice the similarity in CV shapes of the 50 and 500 cycles **(Figure S1)**. Moreover, a pronounced colour change is observed upon cycling. During the reductive scan the initially dark green VO_2 film turns green then blue and finally, after the (re)oxidation process, orange (**Figure 3b**).

The switching optical response in between alternating potentials is one of the most important characteristics of electrochromic materials and devices. The switching times, defined as the time required to reach 90% of the full response, were estimated to 5 and 7 s from chronoamperometry measurements performed at -0.9 V (reduced state) and +1.9 V (oxidized state) for 30 sec., respectively **(Figure 3c)**. The response times, slightly higher in the reduction process (7 s) than in the oxidation one (5 s), are probably due to the transition from a more conductive to less conductive state, in agreement with the existence of various vanadium oxidation states in the reduced state.

The diffuse reflectance spectra of vanadium dioxide films for the oxidized and reduced states are illustrated in **Figure 4a**. The color switching between the blue-reduced and the orange-oxidized state corresponds to reflectance values of about 5% and 55% at 610 nm, respectively, leading to an optical reflectance modulation, ΔR, of about 50%.

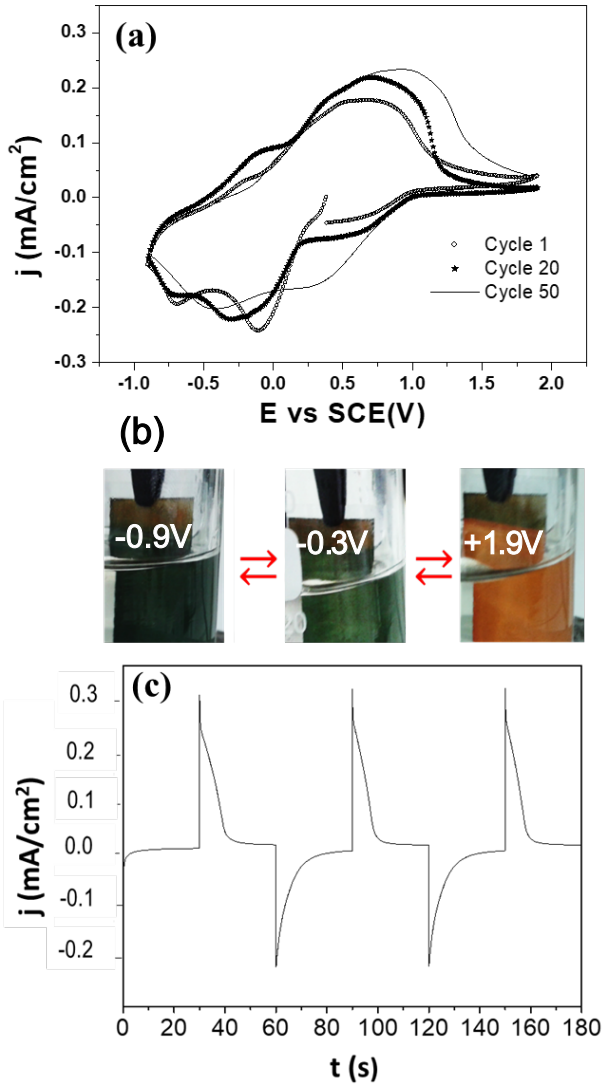

Figure 3. (a) Evolution of the cyclic voltammograms (1, 20 and 50 cycles) of VO_2(M1) film cycled in Pt/LiTFSI-EMITFSI/VO_2 vs SCE with a 10 mV/s scan rate, (b) visual appearance of the films in different color states and (c) Chronoamperograms at -0.9 V (reduced state) and +1.9 V (oxidized state) for 30 s.

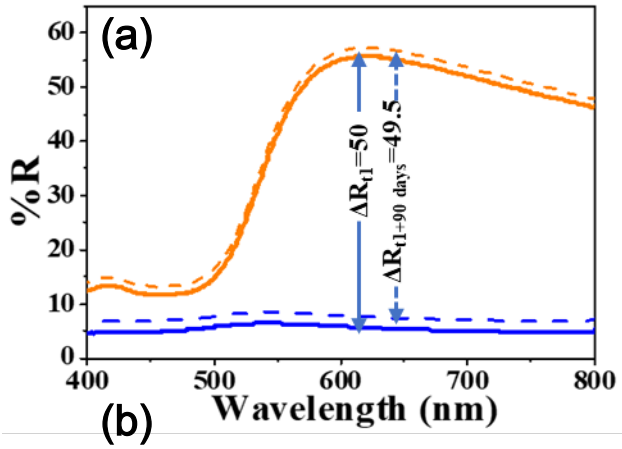

(b)

VO_2	L*	a*	b*
As-dep	16	-2	2
-0.3 V	29	-19	44
-0.9 V	19	-13	-19
+1.9 V	71	27	41

Figure 4. (a) *Ex-situ* diffuse reflectance of VO_2(M1) films in reduced blue state at (−0.9 V) and oxidized orange state (+1.9 V). Dashed lines represent the diffuse reflectance spectra recorded after three months storage under ambient air at room temperature (b) L*a*b parameters of VO_2 in different colored states.

The coloration efficiency (CE), defined as the change in optical density (OD) per unit charge density (Q) was calculated from the following formula:

$$CE = \Delta OD/Q \qquad eq\ (1)$$

Where $OD = \log(R_{ox}/R_{red})$, Q the electrochemical capacity per unit area, R_{ox} the reflectance at the oxidized state and $R_{red.}$ the reflectance at the reduced state. The coloration efficiency is thus estimated to 56 cm^2/C.

The L*a*b* parameters, extracted from the diffuse reflectance curve (not shown here) are illustrated in **Figure 4b.** The L*a*b* parameters are in good agreement with the visual colors. Indeed, for the blue-reduced state (at −0.9 V), the L*a*b* parameters are 19, −13, and -19, respectively, whereas for the orange-oxidized state (at 1.9 V), the L*a*b* parameters are 71, 27, and 41, respectively. Using eq(2), these values lead to a color contrast ΔE* = 88.

$$\Delta E^* = [(\Delta L^*)^2 + (\Delta a^*)^2 + (\Delta b^*)^2]^{1/2} \qquad eq\ (2)$$

Where $\Delta L^* = |L^*_2 - L^*_1|$, $\Delta a^* = |a^*_2 - a^*_1|$ and $\Delta b^* = |b^*_2 - b^*_1|$

In addition, **Figure 4a** shows the reflectance spectra of the oxidized and reduced states for films stored 3 months under ambient air at room temperature with no electrical voltage applied. In agreement with similar apparent colors and visual aspects, the reflectance curves for each color state are rather the same after three months, confirming the strong memory effect of the vanadium oxide films. Such property allowed us to investigate the electrochromic mechanism by performing *ex-situ* characterization of the films at various states using a combination of techniques.

Preliminary Mechanism

The mechanism at the origin of the multi-electrochromism in VO_2(M1) relies both on structural and electronic evolutions. The Grazing Incidence X-Ray Scattering (GISAXS) pattern of the as-deposited film unambiguously corresponds to monoclinic VO_2 (M1) (Space Group: P21/c) whereas the GISAXS patterns of the films recovered at the green and blue reduced states after 50 cycles exhibit mainly broad diffraction lines due to amorphous phases (**Figure 5a and b**). In oxidative regime (+1.9 V; **Figure 5c**), leading to an orange coloration, the peaks can be indexed as highly crystallized orthorhombic V_2O_5 (SG: Pmmn) with a pronounced orientation along the (001) crystallographic direction. Interestingly, such evolution was already reported for V_2O_3 films demonstrating, for both oxide stoichiometries, the trend to an irrevsrible transformation to the most thermodynamically stable V_2O_5[22].

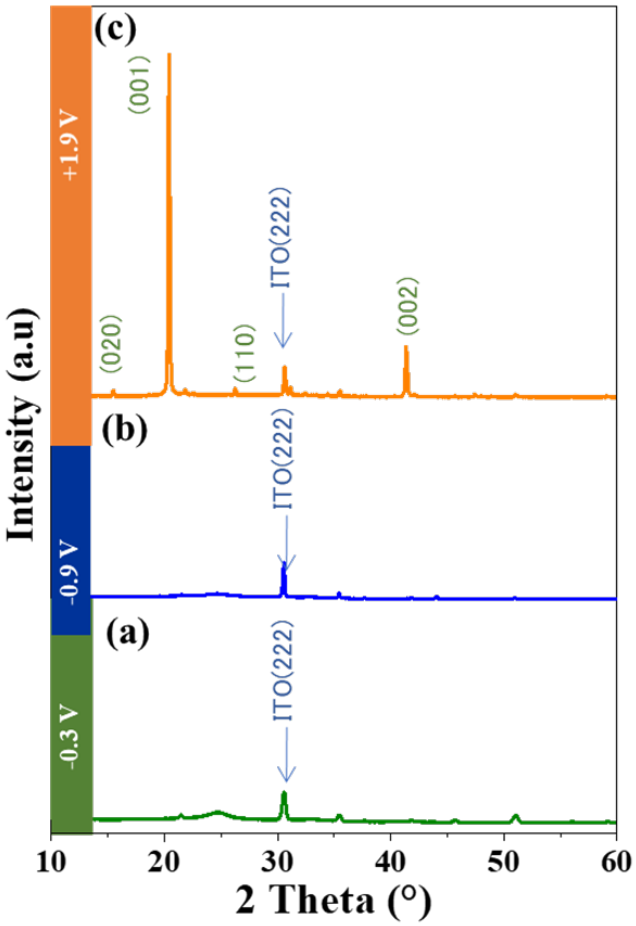

FIGURE 5. *Ex-situ* Grazing Incidence XRD patterns of VO_2 after 50 cycles at reduced green state (a), reduced blue state (b) and oxidized orange state (c). Peaks, ITO substrate are indocated.

The GISAXS results were combined with TEM. **Figure 6** shows the morphology and the crystallites size for each colored state. As for the film before cycling (Figure 2b,c), the film reduced at -0.3V shows a veil-shaped morphology (**Figure 6a**). For the reduced blue state (-0.9V), a drastic change is observed with the appearance of agglomerated particles (**Figure 6b**). Furthermore, for the re-oxidized orange state (+ 1.9 V), the film appears homogenous with well-faceted particles **(Figure 6c)**. This surprising morphological evolution is associated with structural changes as evidenced the electron diffraction pattern. For the reduced green state (-0.3V), the selected area electron diffraction SAED image still reveals the presence of some spots related to the VO_2 monoclinic phase **(Figure 6d)**. At -0.9 V, the reduced blue film is characterized by the presence of several spots characteristic of the V_2O_3 phase while the re-oxidized (+1.9V) orange film exhibits a SAED pattern characteristic of the V_2O_5 phase. At this stage, the identification of the blue state with the V_2O_3 phase remains unexpected as further discussed in respect of the electrochemical capacity value as well as the

overall modification of the vanadium oxidation states using various characterizations.

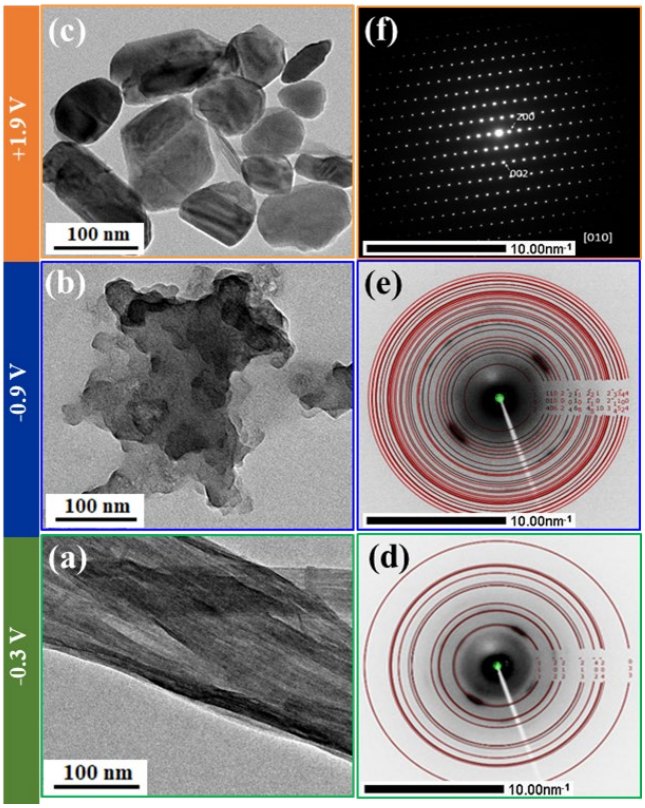

FIGURE 6. High-resolution TEM images of VO_2 film after 50 cycles at reduced green state (a), reduced blue state (b), and reoxidized orange state (c) and corresponding SAED patterns, d, e, f.

Further insights in the structural evolution upon cycling were investigated by Solid-state NMR spectroscopy. ^{7}Li and ^{51}V MAS NMR experiments were conducted on scratched films recovered at different states (reduced at -0.3 V and -0.9 V and re-oxidized at +1.9 V).

As expected for both reduced films, strong interactions with paramagnetic V^{4+} ions prevent the observation of any ^{51}V NMR signals, except for a very weak signal with isotropic shift $\delta_{iso} \approx$ -590 ppm. The shape of the spinning sideband pattern suggests a large chemical shift anisotropy (CSA) ($\delta_\sigma \approx 750$ ppm and $\eta_\sigma \approx 0.2$) related to significant distortion of the vanadium site. Similar values of isotropic shifts and CSA parameters were reported for ^{51}V MAS NMR signals observed for $CeVO_4$[25] and various other vanadium oxides or oxysulfates[26] where vanadium ions are located at distorted octahedral sites associated in V-O-V chains. However, the very low intensity of the ^{51}V NMR signals observed for the reduced VO_2 films (figure 7) and poor signal over noise ratio do not allow us to accurately determine the values of CSA and quadrupolar parameters (δ_σ, η_σ, C_Q, η_Q) and then undoubtedly associated this resonance signal with some V^{5+} ions in isolated and distorted V-O-V chains[25,26]. On the contrary, the ^{51}V NMR spectrum of the reoxidized film exhibits an intense and sharp signal (**Figure 7b**) characteristic of ^{51}V in a well-crystalized V_2O_5 phase, in good agreement with the *ex-situ* grazing incidence XRD results (**Figure 5**).

Regarding the Li^+ ions environment within the reduced (lithiated) VO_2 films, the ^{7}Li NMR spectra (**Figure 7a**) show two main resonance lines at -0.8 ppm and -21.4 ppm consistent with those already reported in previous studies for chemically or electrochemically lithium intercalated $Li_xV_2O_5$ compounds [27-30].

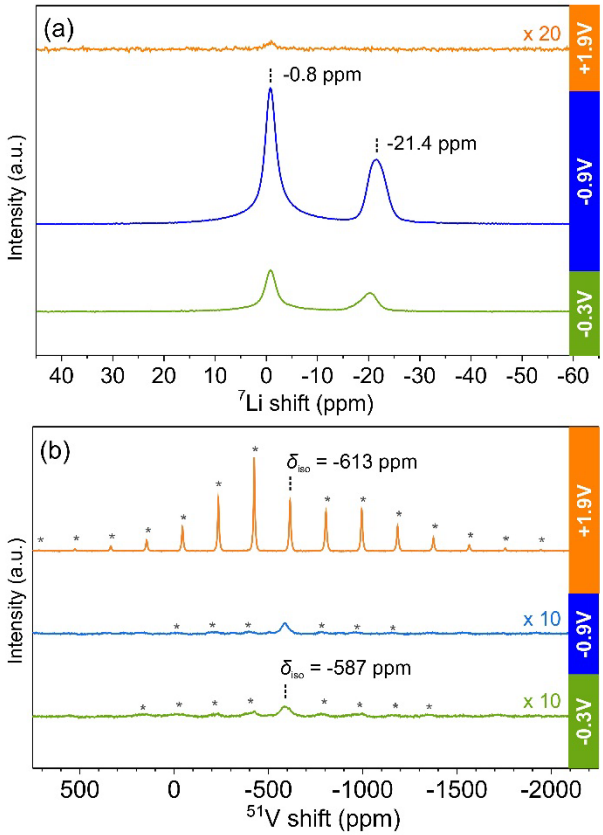

FIGURE 7. (a) ^{7}Li MAS-NMR spectra ($B_0 = 7.1$ T, $\nu_r = 30$ kHz) and (b) ^{51}V MAS-NMR spectra ($B_0 = 11.7$ T, $\nu_r = 25$ kHz) of VO_2 films at reduced-green state, reduced blue state and re-oxidized orange state, 50 cycles. (* spinning side bands)

Asai *et al.* have shown that depending on the lithiation rate of amorphous $Li_xV_2O_5$, Li^+ ions can actually occupy three different sites within the large cavity formed by eight VO_5 square pyramids[31]. For the reduced VO_2 films, the two observed ^{7}Li NMR resonance lines can then be associated with Li ions at distinct locations within the vanadium oxide structure. Both signals are characterized by a short spin-lattice relaxation time ($T_1 < 100$ ms), revealing magnetic interactions between the Li nuclear spins and the unpaired electronic spins of paramagnetic ions (V^{4+} or VO^{2+}). The NMR signal with ^{7}Li shift close to 0 ppm is attributed to Li ions located at octahedral sites similar to those occupied by Li in electrochemically intercalated $Li_xV_2O_5$ with $x \leq 1$[32].The signal observed at about -21 ppm is actually the sum of two distinct resonance lines, as evidenced by NMR experiments performed at various MAS rates. The isotropic shift value and its variation with the MAS rate and then

with temperature (due to frictional heating of the rotor) suggests that the Li ions responsible for these resonance lines are close to paramagnetic centres (Fermi contact or pseudocontact interaction). Thus, several Li local environments were clearly evidenced by ^{7}Li NMR. Moreover, the intensity of all ^{7}Li NMR signals increases as the potential decreases from -0.3 V to -0.9 V (**Figure 7a**), supporting the effective lithiation of the VO_2 film. The ^{7}Li NMR spectrum of the reoxidized (delithiated) film (recovered at +1.9 V) only shows a very weak signal

in the structure (small irreversible capacity loss) or some electrolyte residue located at the film surface.

Aside from the structural modifications, redox reactions associated with the modulation of the vanadium oxidation states were evaluated by various techniques starting with XPS analysis. To identify the valence state, the binding energy of vanadium was determined. V2p$_{3/2}$ core peak spectra were recorded for the as-deposited film and at specific potentials corresponding to distinct colorations **(Figure 8)**: the green intermediate reduced state, the blue reduced state and the orange oxidized state, recorded after 50 cycles. In the potential range from +1.9 to −0.9 V, only two V2p$_{3/2}$ core peaks are identified. The orange coloration being associated with the occurrence of a main peak near 517.3 eV assigned to V^{5+} ions. The second peak centered at 516.1 eV is ascribed to the V^{4+} ions. As expected, this contribution is predominant in the as-deposited film while V^{5+} ions are also present due to surface oxidation. The attribution of the 516.1 eV can be contested as this peak could be indeed the convolution of the characteristic signals of both V^{3+} and V^{4+} ions. The V^{5+}/V^{4+} ratio shows that, whatever the coloration state, vanadium ions always have mixed 5+ and 4+ valence states. After 50 cycles, for a green color at -0.3 V, the V^{5+}/ V^{4+} ratio is in favor of the V^{5+} ions with a significant minor peak of V^{4+} signal; this ratio is approximately around the unit, i.e. showing the same proportion of V^{5+} and V^{4+} ions, for the reduced blue state at -0.9 V. For the return sweep, in oxidative regime up to 1.9 V, leading to an orange color, the V^{5+} ions are at the origin of almost the entire XPS spectrum. The XPS results confirm the XRD study showing the re-oxidation to the stable V_2O_5 with orange color.

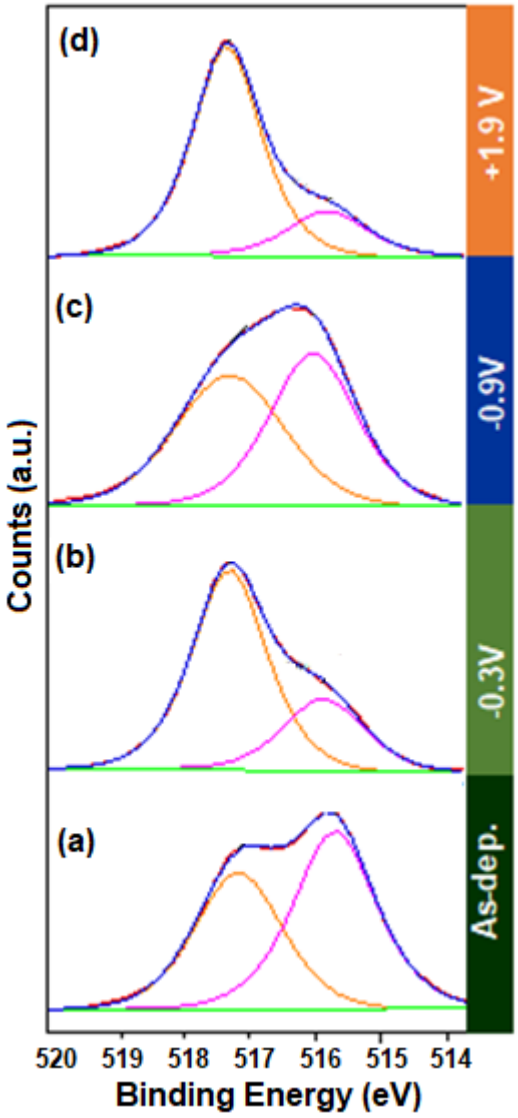

FIGURE 8. *Ex-situ* XPS spectra of VO_2 films as deposited (a), reduced blue state at -0.3V (b), reduced blue state at -0.9V (c), and reoxidized orange state (d). Fitting of the V2p3/2 core peak spectra showing two main contributions in orange and pink centered near 517.3 eV and 516.1 eV, respectively.

The variation of vanadium oxidation state upon cycling was also clearly evidenced by EPR measurements performed on scratched films at different states (reduced at -0.3 V and -0.9 V and reoxidized at +1.9 V). The EPR powder spectra **(Figure 9)**

mainly exhibit an axial signal with g values $g_{\perp} = 1.98$ and $g_{//} = 1.91$ associated with paramagnetic V^{4+} ($3d^1$) or vanadyle $(V = O)^{2+}$ cations[33,34]. This EPR signal clearly increases between -0.3 V and -0.9 V indicating the partial reduction of V^{5+} ions. Moreover, for the sample recovered at -0.3 V an additional signal is detected. This last signal, which is characterized by an hyperfine structure (marked by stars in **Figure 9**) due to unpaired electron spin interaction with the ^{51}V nuclear spin ($I = 7/2$), reveals the presence of isolated (oxo)vanadium(IV) ions[35,36]. Upon reduction, the concentration in paramagnetic vanadium ions increases and no hyperfine structure is observed because of strong exchange interactions between the unpaired electron spins. After reoxidation (at +1.9 V), both EPR signals are still detected but their intensities are significantly reduced in good agreement with ^{51}V NMR and XPS analyses showing that vanadium is mainly at the +5 oxidation state.

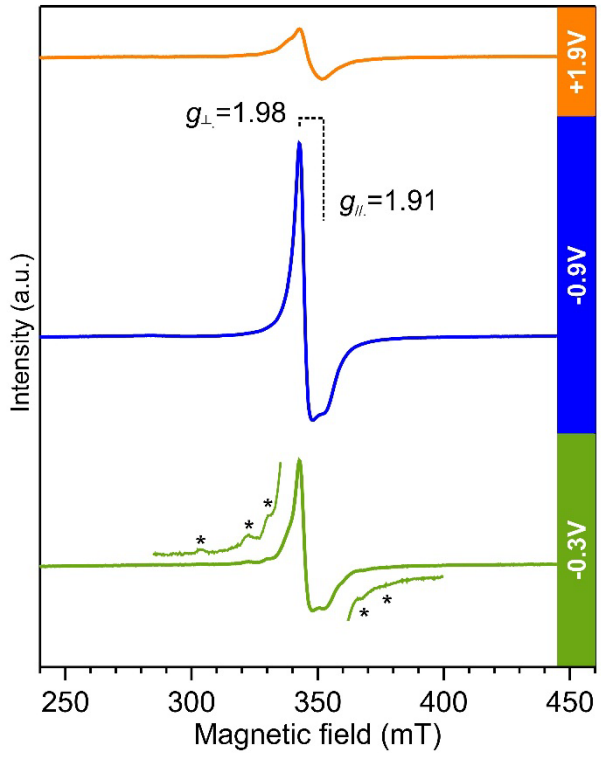

FIGURE 9. Room temperature X-band EPR spectra of VO_2 films at different states. * ^{51}V ($I = 7/2$) hyperfine structure.

EELS was also carried out to characterize the VO_2 thick films at different colour states. **Figure 10** presents the EELS spectra of the VO_2 at reduced and oxidized states. In EELS characterization, V-L_3 and V-L_2 edges reflect the excitations from the $V2p_{3/2}$ and $V2p_{1/2}$ core levels to the unoccupied V3d states, while the O-K band is due to the excitation of the O1s electrons[37-39]. The difference in the oxidation state of vanadium atoms results in the chemical shifts of the V-L_3, V-L_2 and O1s edges. To obtain the insight into the extent of these shifts, the EELS spectra of standard compounds for V_2O_5, VO_2 and V_2O_3 powders were first measured **(Figure S4)**. Their comparison indicates the tendency of V-L_3 and V-L_2 absorption edge onset energies to increase with the increasing oxidation state of vanadium cations. Upon normalization to V-L_3 absorption edge, it became evident that the relative V-L_3/V-L_2 intensity ratio decreased with the increase in oxidation state of vanadium **(Figure 10)**. A characteristic feature is also the shape and intensity of O1s pre-edge, being much more intense for higher oxidation state of vanadium[40]. From literature, the shift ΔE of the V-L_3 edge relative to the O-K peak as measurement of oxidation state was chosen. ΔE decreases from 13.8 eV (-0.9V), to 13.2 eV (-0.3 V) and 12.2 eV (+1.9 V) in agreement with the presence of mixed states in reduced states and V^{5+} in oxidized ones.

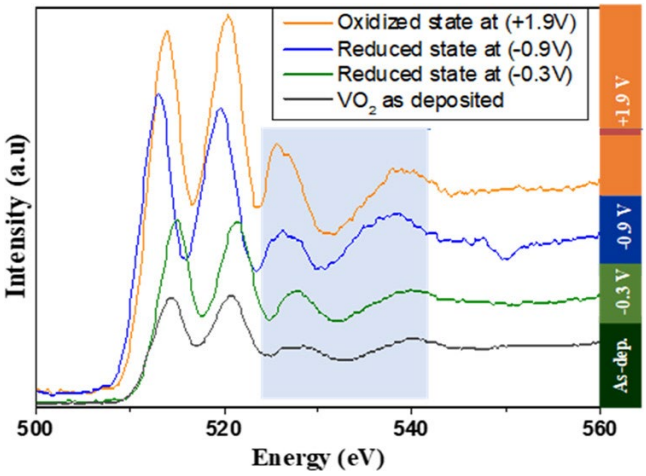

FIGURE 10. EELS spectra of VO_2 film as-deposited and after 50 cycles at reduced green state, reduced blue state and oxidized orange state. V-L_3 / (513 eV), V-L_2 / (520 eV) and O-K; (526 eV) Blue region highlighted. For each spectrum, the peak intensity is linked to the thickness of the scratched film and thus remains arbitrary for the comparison.

CONCLUSION

Electrochromism starting from opaque VO_2 greenish films is reported. Upon cycling in lithium based electrolyte, a progressive reversible switch from orange in oxidized state to blue in the reduced state takes place. The strong memory effect, associated with the persistence of the blue coloration in the reduced state allowed a careful characterization using techniques including Li and V NMR, XPS, leading to the conclusion of an initial and irreversible transformation to V_2O_5. The combination of the various techniques highlights the complexity of the mechanism based on the oxydo-reduction of the vanadium cations. This study represents an initial contribution to the understanding of the electrochromic mechanism taking place in vanadium oxide films giving rise to desirable multichromism and rather unique strong memory effect in oxides. As it was previously reported for V_2O_3[22], one can extend that whatever the initial oxide stoichiometry the trend is an irreversible transformation to the most thermodynamically stable V_2O_5 phase upon cycling.

Supporting Information: "500 Cyclic voltammograms (OPJ), cycling stability (OPJ), reflectance (OPJ) and EELS (OPJ) spectra of powders used as references"

Acknowledgements: The authors wish to thank François Weill for fruitful HRTEM discussions.

Author contributions:

Issam Mjejri: conceptualization, characterization, writting. Mathieu Duttine: NMR, EPR characterizations, writting. Sonia Buffière: TEM, EELS characterizations, writing. Christine Labrugère XPS characterization, writting: Aline Rougier: supervision. All authors contributed to the discussions and revisions of the manuscript.

Competing financial interests

The authors declare no competing financial interests.

References

(1) Keersmaecker M.D.; Lang A.W.; Österholm A.M.; Reynolds J.R., All polymer solution processed electrochromic devices: a future without indium tin oxide?, *ACS Appl Mater. Interfaces* **2018,** 10, 31568–31579.

(2) Wen R.T.; Malmgren S.; Granqvist C.G.; Niklasson G.A., Degradation dynamics for electrochromic WO_3 films under extended charge insertion and extraction: unveiling physicochemical mechanisms, *ACS Appl. Mater. Interfaces* **2017**, 9, 12872–12877.

(3) Granqvist C. G.; Arvizu M.A.; Qu H.; Wen R; Niklasson G. A., Advances in electrochromic device technology: multiple roads towards superior durability. *Surf. Coat. Technol.* **2019**, 357, 619–625

(4) Hassab, S.; Shen, D. E.; Österholm, A. M.; Da Rocha, M.; Song, G.; Alesanco, Y.; Viñuales, A.; Rougier, A.; Reynolds, J. R.; Padilla, J. A New Standard Method to Calculate Electrochromic Switching Time. *Sol Energy Mater Sol Cells* **2018**, *185*, 54–60.

(5) Tällberg R.; Jelle B. P.; Loonen R.; Gaoa T.; and Hamdy M., Comparison of the energy saving potential of adaptive and controllable smart windows: A state-of-the-art review and simulation studies of thermochromic, photochromic and electrochromic technologies, *Sol. Energy Mater. Sol. Cells,* **2019**, 200, 109828-109857.

(6) Costa C.; Pinheiro C.; I. Henriques I.; Laia C. A. T., Inkjet Printing of Sol–Gel Synthesized Hydrated Tungsten Oxide Nanoparticles for Flexible Electrochromic Devices. *ACS Appl. Mater. Interfaces* **2012**, 4, 3, 1330–1340.

(7) Zhang G.; Guo K; Shen X.; Ning H.; Liang H.; Zhong J.; Xu W.; Tang B.; Yao R.; Peng J. Physical Simulation Model of WO_3 Electrochromic Films Based on Continuous Electron-Transfer Kinetics and Experimental Verification. *ACS Appl. Mater. Interfaces* **2021**, 13, 3, 4768–4776.

(8) Luo Z.; Liu L.; Yang X.; Luo X.; Bi P.; Fu Z.; Pang A.; Li W. ; Yi Y. Revealing the Charge Storage Mechanism of Nickel Oxide Electrochromic Supercapacitors. *ACS Appl. Mater. Interfaces* **2020**, 12, 35, 39098-39107.

(9) Chen J. Z.; Ko W.-Y.; Yen Y.-C.; Chen P.-H.; Lin K.-J. Hydrothermally Processed TiO_2 Nanowire Electrodes with Anti reflective and Electrochromic Properties. *ACS Nano* **2012**, 6, 8, 6633-6639.

(10) Mjejri I.; Grocassan R.; Rougier A., Enhanced Coloration for Hybrid Niobium-Based Electrochromic Devices. *ACS Appl. Energy Mater.* **2018**, 1, 4359−4366.

(11) Novak T. G.; Kim J.; Tiwari A. P.; Kim J.; Lee S.; Lee J.; Jeon S.. 2D MoO_3 Nanosheets Synthesized by Exfoliation and Oxidation of MoS_2 for High Contrast and Fast Response Time Electrochromic Devices. *ACS Sustainable Chemistry & Engineering* **2020,** 8, 30, 11276-11282.

(12) Kovendhan M.; Joseph P.-D.; Manimuthu P.; Sendilkumar A.; Karthick S.N.; Sambasivam S.; Vijayarangamuthu K.; Kim H.J.; Choi B.C.; Asokan K.; Venkateswaran C.; Mohan R. Prototype electrochromic device and dye sensitized solar cell using spray deposited undoped and 'Li' doped V_2O_5 thin film electrodes, *Curr. Appl. Phys.* **2015**, 15, 622–631.

(13) Armer C.F.; Yeoh J.S.; Li X.; Lowe A., Electrospun vanadium-based oxides as electrode materials, *J. Power Sources* **2018**, 395, 414–429.

(14) Xiong C.; Aliev A.E.; Gnade B.; Balkus K.J., Fabrication of Silver Vanadium Oxide and V_2O_5 Nanowires for Electrochromics, *ACS Nano*, **2008** 2(2) 293 – 301.

(15) Tutel Y. ; Batuhan Durukan M. ; Koc S.; Koylan S.; Cakmak H.; Kocak Y. ; Hekmat F.; Ozensoy E. ; Ekmel Ozbay E.; Arslan Udum Y.; Toppare L.;, and Emrah Unalan H. Multichromic Vanadium Pentoxide Thin Films Through Ultrasonic Spray Deposition, *J. Electrochem. Soc.* **2021**, 168 106511

(16) Tong Z.; Li N.; Lv H.; Tian Y.; Qu H.; Zhang X.; Zhao J.; Li Y. Annealing synthesis of coralline V_2O_5 nanorodarchitecture for multicolorenergy-efficient electrochromicdevice *Sol Energy Mater Sol Cells* **2016**, 146, 135-143

(17) Qazilbash M.; , M. Brehm M.; Chae B.G.; Ho P.C.; Andreev G.O.; Kim B.J.; Yun S.J.; Balatsky A.V.; Maple M.B.; Keilman F., Mott transition in VO_2 revealed by infrared spectroscopy and nano-imaging. *Science*, **2007,** 318, 1750-1753.

(18) Popuri S.R. ; Artemenko A. ; Decourt R.; Villesuzanne A.; Pollet M. Presence of Peierls pairing and absence of insulator-to-metal transition in VO_2 (A), a structure-property relationship study. *Phys. Chem. Chem. Phys.*, **2017**, 19, 6601-6609.

(19) Victor, J.L.; Marcel, C.; Sauques, L.; Penin, N.; Rougier A. High quality thermochromic VO_2 thin films deposited at room temperature by balanced and unbalanced HiPIMS. *Sol Energy Mater Sol Cells*, **2021**, 227, 111113-111121.

(20) Khan M.-S.-R.;, Khan K.-A.; Estrada W.; Granqvist C.-G. Electrochromism and Thermochromism of Li_xVO_2). *Journal of Applied Physics* **1991**, 69, 3231-3234.

(21) Mjejri I.; Rougier A.; Gaudon M. Low-cost and facile synthesis of the vanadium oxides V_2O_3, VO_2, and V_2O_5 and their magnetic, thermochromic and electrochromic properties, *Inorg. Chem.* **2017**, 56, 1734–1741.

(22) Mjejri I.; Gaudon M.; Song G.; Labrugère C.; Rougier A. Crystallized V_2O_5 as oxidized phase for unexpected multicolor electrochromism in V_2O_3 thick films. ACS Appl. Ener. Mater., **2018**, 1(6), 2721-2729.

(23) Gonçalves A.; Resende J.; Marques A.-C.; Pinto J.-V.; Nunes D.; Marie A.; Goncalves R.; Pereira L.; Martins, R.; Fortunato E. Smart optically active VO_2 nanostructured layers applied in roof-type ceramic tiles for energy efficiency *Sol Energy Mater Sol Cells* **2016**, 150, 1-9,

(24) Xiao X.; Zhang H.; Chai G.; Sun Y.; Yang T.; Cheng H.; Chen L.; Miao L.; Xu G. A cost-effective process to prepare VO_2 (M) powder and films with superior thermochromic properties. *MATER RES BULL*, **2014**, 5, 6-12.

(25) Matta J.; Courcot D.; Abi-Aad E.; Aboukais A. Identification of Vanadium Oxide Species and Trapped Single Electrons in Interaction with the $CeVO_4$ Phase in Vanadium-Cerium Oxide Systems. ^{51}V MAS NMR, EPR, Raman, and Thermal Analysis Studies. *Chem. Mater.* **2002**, 14, 4118-4125.

(26) Lapina O.B.; Khabibulin D.F.; Shubin A.A.; Terskikh V.V. Practical aspects of ^{51}V and ^{93}Nb solid-state NMR spectroscopy and applications to oxide materials. *Progress in Nuclear Magnetic Resonance Spectroscopy* **2008**, 53, 128-191.

(27) Cocciantelli J. M.; Suh K. S.; Sénégas J.; Doumerc J. P.; Soubeyroux J. L.; Pouchard M.; Hagenmuller P.. ^7Li NMR in Electrochemically intercalated γ-$Li_xV_2O_5$ Bronzes ($0.95 \leq x \leq 1.9$). *J. Phys. Chem. Solids* **1992,** 53(1), 51-55.

(28) Cocciantelli J.M.; Suh K.S.; Sénégas J.; Doumerc J.P.; Pouchard M. ^7Li NMR of Electrochemically Inserted $Li_xV_2O_5$. *J. Phys. Chem. Solids* **1992**, 53(1) 57-59.

(29) Stallworth P.E.; Johnson F.S.; Greenbaum S.G.; Passerini S.; Flowers J.; Smyrl W.; Fontanella J.J. Magnetic resonance studies pf chemically intercalated $Li_xV_2O_5$ (x=1.16 and 1.48). *Solid State Ionics* **2002**, 146, 43-54.

(30) Nakamura K.; Nishioka D.; Michihiro Y.; Vijayakumar M.; Selvasekarapandian S.; Kanashiro T. ^7Li and ^{51}V NMR Study on Li^+ Ionic Diffusion in Lithium Intercalated $Li_xV_2O_5$. *Solid State Ionics* **2006**, 177, 129-135.

(31) Asai T.; Sugimoto S.; Kawai S.; Okada S.; Yamaki J.-I. NMR Study on the Li Diffusion in a Cathode Material of Amorphous Vanadium Pentoxide-5 mol% Phosphorous Pentoxide. *Mat. Res. Bull.* **1989**, 24, 75-82.

(32) Fu R.; Ma Z.; Zheng J.; Au G.; Plichta E.J.; Ye C. High-Resolution ^7Li Solid-State NMR Study of $Li_xV_2O_5$ Cathode Electrodes for Li-Rechargeable Batteries. *J. Phys. Chem. B* **2003**, 107, 9730-9735.

(33) Pecquenard B.; Gourier D.; Baffier N. EPR identification of $Li_xV_2O_5$ phases generated by chemical and electrochemical lithium intercalation in V_2O_5. *Solid State Ionics* **1995**, 78, 287-303.

(34) Stallworth P.E.; Johnson F.S.; Greenbaum S.G.; Passerini S.; Flowers J.; Smyrl W.; Fontanella J.J. Magnetic resonance studies pf chemically intercalated $Li_xV_2O_5$ (x=1.16 and 1.48). *Solid State Ionics* **2002**, 146, 43-54.

(35) Schreckenbach J.P.; Strauch P. Microstructure study of amorphous vanadium oxide films. *Appl Surf Sci* **1999**, 143, 6-10.

(36) Gourier D.; Tranchant A.; Baffier N.; Messina R. EPR study of Electrochemical Lithium Intercalation in V_2O_5 Cathodes. *Electrochimica Acta* **1992**, 37, 2755-2764.

(37) Laffont L.; Wu M.Y.; Chevallier F.; Poizot P.; Morcette M., High Resolution EELS of Cu-V oxides: application to batteries materials, Micron 2006, 37, 459-464

(38) Gallasch T. Stockhoff T. Baither D.; Schmitz G., Ion beam sputter deposition of V_2O_5 thin films. *J Power Sources* **2011**, 196, 428-435

(39) Su D. S.; Wieske M.; Beckmann E.; Blume A.; Mestl G.; Schlögl R. Electron Beam Induced Reduction of V_2O_5 studied by Analytical Electron Microscopy. *Catalysis Letters*, **2001**, 75, 1/2, 81-86

(40) Hebert C.; Willinger M.; Su D.-S.; P. Pongratz P.; SchattSchneider P. and Schlôgl R; Oxygen K-edge in vanadium oxides: simulations and experiments, *Eur. Phys. J. B*, **2002**, 28, 407-414